Dependence of the Boundary Heat Flux Width on Core and Edge Profiles in Alcator C-Mod

S.B. Ballinger[1], D. Brunner[2], A.E. Hubbard[1], J.W. Hughes[1], A.Q. Kuang[1], B. LaBombard[1], J.L. Terry[1], A.E. White[1]

[1] MIT Plasma Science and Fusion Center, Cambridge, Massachusetts, USA
[2] Commonwealth Fusion Systems, Cambridge, Massachusetts 02139
Contact: sballin@mit.edu

Abstract

This work presents new evidence that the heat flux width, λ_q, in the Alcator C-Mod tokamak scales with the edge electron pressure, as observed in the ASDEX Upgrade (AUG) tokamak (D Silvagni *et al* 2020 *Plasma Phys. Control. Fusion* **62** 045015), but the scaling with volume-averaged pressure, $\overline{p}$, from the plasma stored energy, found by Brunner et al. (D Brunner *et al* 2018 *Nucl. Fusion* **58** 094002), is a better predictor of λ_q in Alcator C-Mod than the edge electron pressure. All of these findings, showing λ_q decreasing with increased pressures, imply that a high performance core at high pressure will lead to challenging heat and particle exhaust due to very small λ_q. This concern has led to our significant enlargement of the C-Mod database with the electron density, temperature, and pressure profile data from the Thomson scattering and electron cyclotron emission diagnostics. Using the C-Mod database augmented with new profile data, we find that λ_q decreases with increasing edge electron pressure as $\lambda_q \propto p_{e,95}^{-0.26}$, similar to results from AUG, and showing the strength of cross-machine comparisons. We also find that $\lambda_q \propto p_{e,\mathrm{core}}^{-0.56}$, consistent with the original finding from C-Mod that the heat flux width scales as $\overline{p}^{-0.48}$ (D Brunner *et al* 2018 *Nucl. Fusion* **58** 094002). The scalings of λ_q with separatrix pressure and gradient scale length are found to match the AUG results qualitatively. The C-Mod scalings with edge plasma quantities have more scatter than the $\overline{p}$ scaling, and, importantly, show different trends for H-modes relative to L- and I-mode. Investigating the source of this discrepancy presents an opportunity for further study that may improve our ability to predict the heat flux width in different confinement scenarios in the pursuit of optimizing core-edge performance in future reactors.

Introduction

In tokamaks, the heat flux width λ_q describes the decay length of the parallel heat flux into the scrape-off layer (SOL). λ_q is typically inferred by analysis of the heat flux to the divertor target and subsequent magnetic mapping of the profile from the target to the outboard midplane. The target heat flux is obtained using infrared thermography, embedded thermocouples, or Langmuir probe measurements. The mapped profiles are fit with a parametric function. A small value of λ_q results in challengingly large heat fluxes to the divertor, which, if not mitigated, can result in unacceptable sputtering and melting of plasma-facing components. Empirical databases and power law fits are a common technique in fusion research to project parameters to new devices, lacking validated theoretical or first-principles ways of doing so. A multi-machine study by Eich et al. [1] found that λ_q scales approximately as the inverse of the poloidal magnetic field B_p measured at the outer midplane separatrix for plasmas with H-mode confinement and with the outer divertor "leg" attached to the divertor target. This scaling predicts $\lambda_q < 1$ mm for ITER and SPARC [2,3], for plasmas in which ~100 MW (ITER) [1] and ~28 MW (SPARC) of power is foreseen to reach the scrape-off layer [3]. Study of an extensive Alcator C-Mod database found that the average pressure from stored energy ($\overline{p} =$

$2/3\ W_{\mathrm{MHD}}/V_{\mathrm{LCFS}}$, where W_{MHD} is the plasma stored energy and V_{LCFS} is the plasma volume inside the magnetic separatrix, both calculated from EFIT magnetic reconstructions [4]) was an excellent predictor of λ_q with a unified scaling across L-, I-, and H-mode confinement regimes [2]. This implies that high-pressure, high-performance fusion plasmas with conventional magnetic divertor shapes (e.g. the single-null configuration) will likely produce unsustainably high heat flux densities if unmitigated, further motivating the development of solutions such as controlled detachment [5] and advanced divertor configurations such as the super-X [6–9], X-point target [3,7–10], and snowflake divertor [11–13].

A recent study on ASDEX Upgrade (AUG) found a correlation between λ_q and the average pressure, and a stronger correlation between λ_q and the edge electron pressure from Thomson scattering data at $\rho_{\mathrm{pol}} = 0.95$, where $\rho_{\mathrm{pol}} = \sqrt{\Psi_N}$ and $\Psi_N = (\Psi - \Psi_{\mathrm{axis}})/(\Psi_{\mathrm{sep}} - \Psi_{\mathrm{axis}})$ is the normalized poloidal flux. Furthermore, it found that λ_q scales with the electron pressure decay length at the separatrix λ_{pe} and that the data conformed to a relationship of $\lambda_q = 2/7\lambda_{Te}$ between the heat flux width and the separatrix electron temperature decay length as expected in the Spitzer-Härm electron heat conduction regime [14]. It is reasoned that the localized edge pressure and gradients are more directly correlated with the heat flux width than the average pressure. Earlier work on AUG has also verified that profile edge gradients are related to λ_q [15]. The main goal of the present study is to determine whether localized measurements also provide better scalings than the volume-averaged pressure for Alcator C-Mod. A secondary goal is to examine the relationship between edge gradients and the heat flux width in C-Mod.

The unified scalings with average pressure in C-Mod and with average/edge pressure in AUG differ from others in the literature, which tend to be developed for individual confinement modes. Early multi-device studies focused on L-mode [16] and H-mode extrapolations of λ_q to ITER [1,17]. The heuristic drift model performs well for H-modes across several devices but overpredicts λ_q in C-Mod [18,19]. The C-Mod scaling with average pressure has also been tested on a multi-machine L-mode database, which found acceptable cross-device performance that was improved by the inclusion of the inverse aspect ratio a/R_0 and the plasma beta (the study also tested many other L-mode scalings) [20]. The critical gradient model, in which a ballooning instability sets an upper limit on the pressure gradient scale length that is related to the heat flux width, is satisfied on DIII-D but does not provide as good a scaling for λ_q as the heuristic drift model [21,22]. A theory-based scaling for the near SOL pressure decay length in L-mode, however, has been found to be a good predictor of the experimentally measured λ_q in a multi-machine database [23]. Recent studies in H-mode on AUG found that a turbulence control parameter is highly relevant [24] and that filament transport can have a strong impact on λ_q, an effect that is not captured by many of the existing scalings [25]. This underscores the importance of developing empirical scalings for λ_q from databases that cover a wide variety of plasma conditions.

Experimental Setup and Methods

The C-Mod heat flux width database [2] contains fits to the outer divertor heat flux profile for around 300 shots expressing no edge-localized modes (ELMs). In the present work, the original database was narrowed down to around 120 shots that have good core and edge profile data from the Thomson scattering system and stationary plasma conditions over a period of at least 100 milliseconds, resulting in the parameter ranges shown in Table 1. While the database covers a wide range of engineering parameters, the ranges of plasma triangularity and elongation are narrow due to the requirement to sweep the outer strike point over the Langmuir probes and surface thermocouples to measure heat flux profiles on the lower outer divertor target. As in the original database, there are approximately equal proportions of L-mode, I-mode [26], and enhanced D-alpha (EDA) [27] H-mode shots. Approximately half of the L-mode shots are with “forward” toroidal field (i.e. with the ion $B \times \nabla B$ drift toward the X-point and lower divertor) and half are with “reversed” toroidal field. All of the I-mode shots are with reversed field, and all of the EDA H-mode shots are with forward field. No relationship is observed between the heat flux width and the toroidal field direction. The target heat flux profiles are fit using a piecewise sum of exponentials called the multi-λ fit [2] which provides a well-matching shape over the large dynamic range of the probe and thermocouple data, rather than the original parametric

single-λ fit that was used for fitting infrared measurements of divertor heat flux from multiple machines including C-Mod and AUG [1]. One of the quantities obtained from the multi-λ fit, $\lambda_{q,cn}$, describes the falloff in heat flux density in the near common flux region, just as λ_q in the single-λ fit does, so they can be treated the same despite originating from different parametric fits. In this work, the "λ_q" values from C-Mod are actually $\lambda_{q,cn}$.

The C-Mod and AUG databases have some notable differences. The C-Mod database includes higher average pressures and lower values of λ_q than the AUG database: AUG has $3 < \overline{p}/\mathrm{kPa} < 35$ and $0.8 < \lambda_q/\mathrm{mm} < 5$, while C-Mod has $12 < \overline{p}/\mathrm{kPa} < 160$ and $0.6 < \lambda_q/\mathrm{mm} < 2.3$. The C-Mod database also includes a larger range of average pressures for I- and H-mode shots compared to AUG. The AUG database includes inter-ELM periods from ELMy H-modes and ELM-free H-modes, while the H-modes in the C-Mod database are EDA H-modes, which have no ELMs but rather a quasi-coherent edge mode that flushes impurities and particles out of the confined plasma, thereby maintaining a steady-state H-mode [28,29].

Table 1: Parameter ranges for the subset of the C-Mod heat flux width database with good profile data. The poloidal magnetic field is that calculated 1 mm outside the separatrix at the outer midplane.

Parameter	**Range**
On-axis toroidal magnetic field $\boldsymbol{B_T}$ [T]	5.1–7.9
Poloidal magnetic field $\boldsymbol{B_p}$ [T]	0.42–1.3
Average electron density $\boldsymbol{\overline{n}_e}$ [10^{20} m^{-3}]	0.44–4.8
Input power $\boldsymbol{P_{in}}$ [MW]	0.52–5.8
Elongation ($\boldsymbol{\kappa}$)	1.5–1.8
Triangularity ($\boldsymbol{\delta}$)	0.49–0.61

The C-Mod core and edge Thomson scattering diagnostics were used to obtain electron density and temperature data [30]. Electron cyclotron emission (ECE) diagnostics (GPC1 and GPC2) were used to obtain additional electron temperature data [31]. Gaussian process regression (GPR) [32] was used to fit the profiles of density and temperature. Confidence bounds resulting from this method are not rigorous because the Markov chain Monte Carlo (MCMC) method was not used; MCMC can require time-consuming fine tuning which was not feasible for 120 profiles.

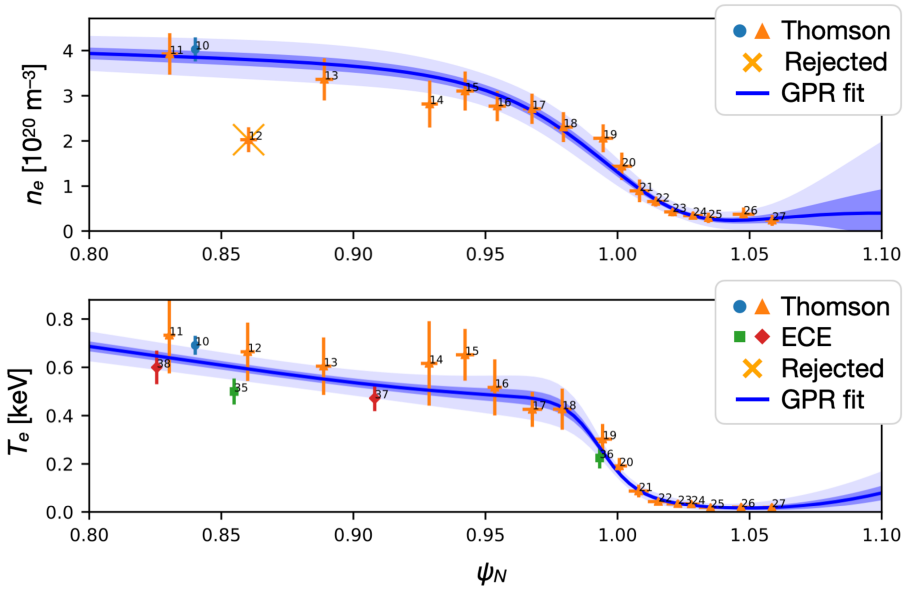

Figure 1: Example of electron temperature and density data and resulting fits from GPR for an H-mode shot (1160729008). The light blue shaded region around the GPR fit shows the confidence bounds.

In order to overcome uncertainty in the location of the separatrix in the Thomson scattering profiles [33,34], the profiles of electron density and temperature obtained from GPR fitting were shifted to have a separatrix temperature consistent with the 2-point model [35]:

$$T_e^{\text{sep}} \approx \left(\frac{7}{16} \frac{P_{\text{sep}} q_{\text{cyl}}^2 A}{\kappa_0^e \, \hat{\kappa} \, \lambda_q} \right)^{2/7}$$

as was done for the AUG profiles [14]. The power crossing the separatrix P_{sep} was approximated as $P_{\text{ICRF}} + P_{\text{OH}} - dW/dt - P_{\text{rad core}}$, where the core radiated power is computed from a foil bolometer array. $q_{\text{cyl}} = \frac{B_t \hat{\kappa}}{\langle B_p \rangle A}$ is the safety factor, where B_t is the toroidal magnetic field at the magnetic axis, $\langle B_p \rangle = \frac{\mu_0 I_P}{2\pi a \hat{\kappa}}$ is the average poloidal magnetic field, $A = R/a$ is the aspect ratio, and $\hat{\kappa} = \sqrt{1 + \kappa^2/2}$, where κ is the elongation. A value of $\kappa_0^e \approx 2000$ (eV)$^{\frac{7}{2}}$ W m^{-1} was used for the Spitzer-Härm electron conductivity. The values of λ_q were those from the database, obtained from fits to the heat flux profile at the outer target. The values of T_e^{sep} obtained using this formalism ranged from 54 to 160 eV.

Results and Discussion

λ_q dependence on edge pressure, density, and temperature

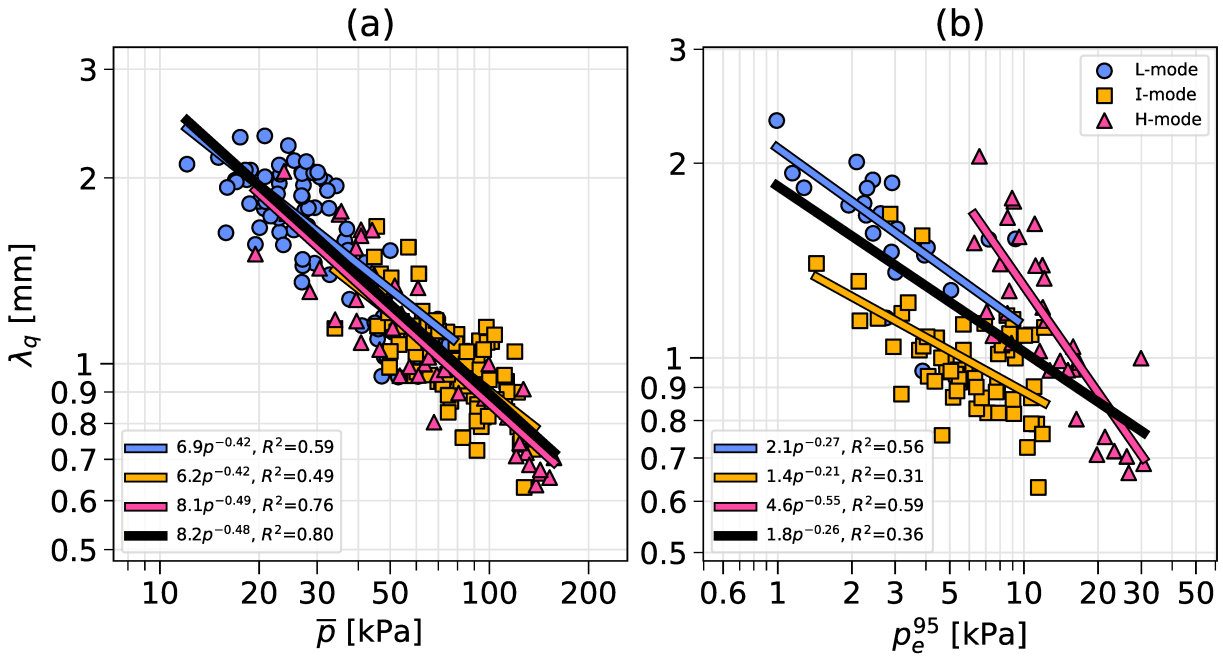

Figure 2: Scalings of the heat flux width with (a) average pressure from stored energy and (b) with electron pressure at $\rho_{pol} = 0.95$ fit with regressions of form $\lambda_q/mm = A(p/kPa)^b$. Fits within individual confinement modes are shown by the correspondingly colored lines, and fits across all confinement modes are shown by black lines.

Figure 2 compares the scaling of λ_q with the average pressure evaluated from the plasma stored energy (Figure 2(a)), and the scaling with the electron pressure at $\rho_{\mathrm{pol}} = 0.95$ ($\Psi_N = 0.90$) from temperature and density profiles (Figure 2(b)). The data are fit with scalings of the form $\lambda_q/\mathrm{mm} = A(p/\mathrm{kPa})^b$, with A and b being the two free parameters output by the fit. There is good agreement between C-Mod and AUG in the scaling of heat flux width with average pressure across all modes: the C-Mod scaling is $\lambda_q/\mathrm{mm} = (8.2 \pm 0.5)(\overline{p}/\mathrm{kPa})^{-0.48\pm0.02}$, while the AUG scaling is $\lambda_q/\mathrm{mm} = (7.6 \pm 0.25)(\overline{p}/\mathrm{kPa})^{-0.52\pm0.01}$ [14]. Both fit factors are very similar, making this a remarkably good cross-regime and cross-device scaling. The fits with electron pressure at $\rho_{\mathrm{pol}} = 0.95$, $\lambda_q/\mathrm{mm} = (2.5 \pm 0.02)(p_e^{95}/\mathrm{kPa})^{-0.34\pm0.01}$ (AUG) [14] and $\lambda_q/\mathrm{mm} = (1.8 \pm 0.1)(p_e^{95}/\mathrm{kPa})^{-0.26\pm0.03}$ (C-Mod) are quite similar. The absolute value of the edge pressure fit exponent is lower than that of the fit with average pressure. There is also considerably more scatter in the edge data, with lower coefficients of determination (R^2) in all cases. Finally, if we separately fit data from L-, I-, and H-mode as a function of p_e^{95}, it is found that the H-mode heat flux width scales as $(p_e^{95})^{-0.55}$, which is quite a different exponent compared to that of the L-modes (-0.27) and I-modes (-0.21). The AUG database has a smaller range of average and edge pressures in H-mode, making it difficult to say whether a separate trend for H-modes is observed in AUG.

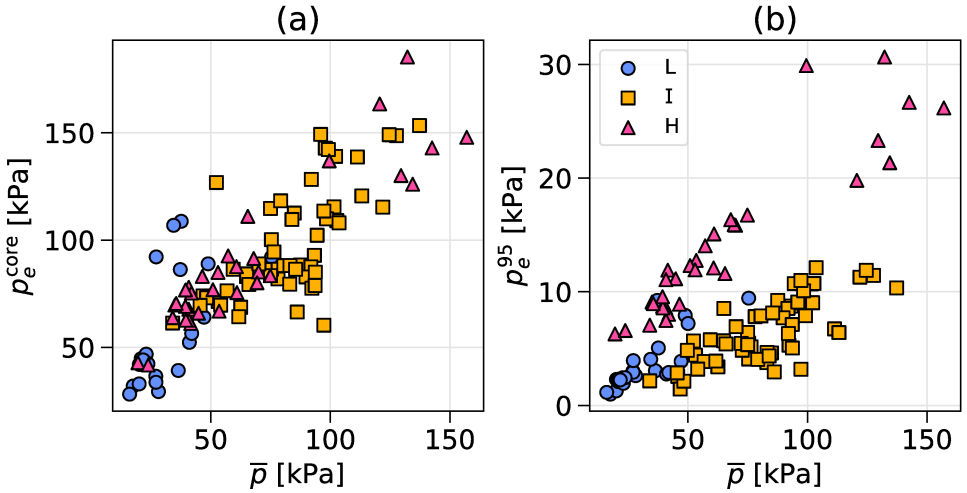

Figure 3: (a) Core ($\rho_{pol} \approx 0.1$) electron pressure as a function of the average pressure from stored energy, and (b) electron pressure at $\rho_{pol} = 0.95$ as a function of the average pressure.

Figure 3(a) shows an approximately linear relationship between core ($\rho_{\mathrm{pol}} \approx 0.1$) electron pressure and average pressure, with all confinement modes obeying a similar trend, but in Figure 3(b) H-modes have clearly higher edge pressure at $\rho_{\mathrm{pol}} = 0.95$ than L- and I-modes. This is expected due to the fact that the majority of H-modes do not have higher core pressure than L- and I-mode shots, but have higher edge pressure due to their higher edge density. This explains why using the edge pressure for regressions in this database leads to different trends for different confinement modes.

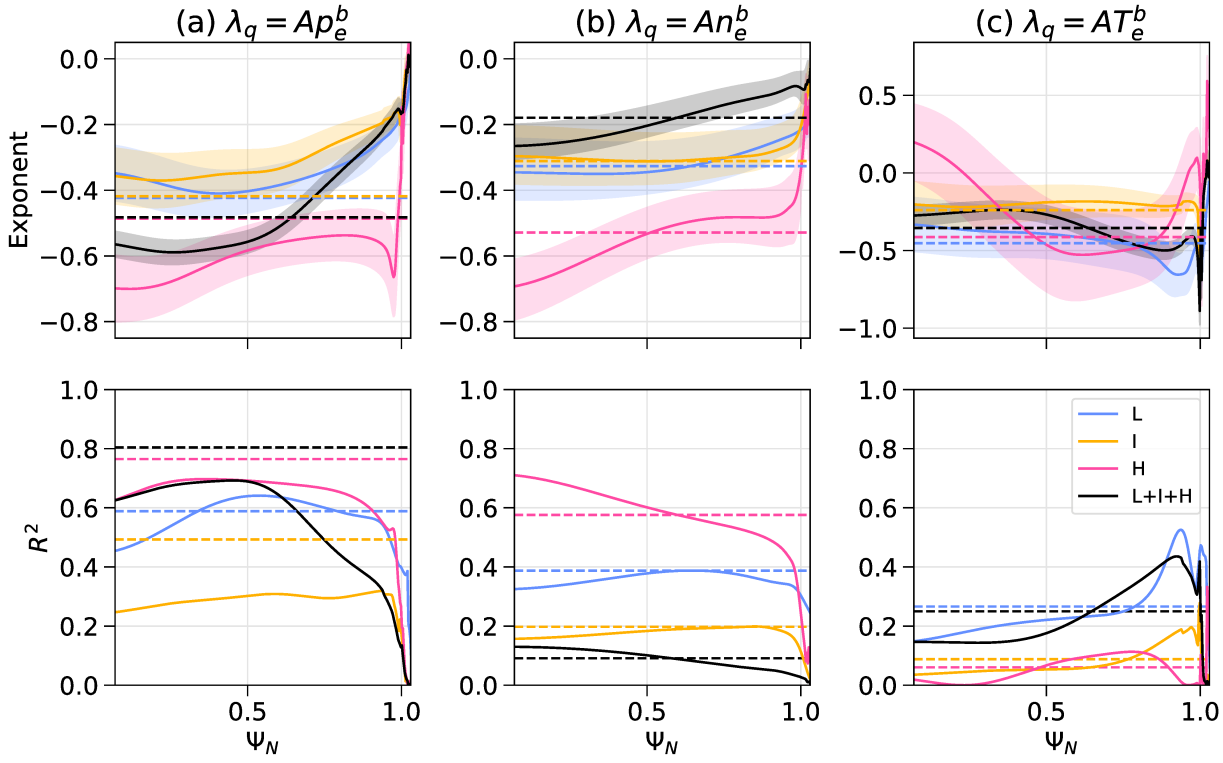

Figure 4: (top row) Exponent obtained from fitting a regression of form $\lambda_q = AX^b$ at each radial coordinate of normalized poloidal flux Ψ_N, with X being the electron pressure (column a), electron density (column b), and electron temperature (column c). (bottom row) Coefficient of determination R^2 for each regression. Colored lines show fits to individual confinement modes, and black lines show fits to all confinement modes. Dashed horizontal lines show exponents and R^2 values for fits to volume-

averaged quantities: average pressure from stored energy (column a), average electron density from profiles (column b), and average electron temperature from profiles (column c).

The large range of average pressures in the C-Mod database across all confinement modes and the availability of profiles of n_e and T_e make it possible to exhaustively evaluate relationships between λ_q and localized plasma parameters. Figure 4 shows regressions of the form $\lambda_q = AX^b$, where X is alternately p_e, n_e, and T_e, and fits are performed at every radial coordinate. Superimposed in dashed horizontal lines are the results of fits using volume-averaged quantities. $\overline{p}$ is obtained from the plasma stored energy while $\overline{n}_e$ and $\overline{T}_e$ are obtained by integrating profiles from Ψ_N of 0 to 1, with no T_e^{sep}-based shifting to avoid having to extrapolate profiles in case of an outward shift (note that the T_e^{sep}-based shifting impacts the average values much less than local values). The graphs show Ψ_N up to 1.03, past which the experimental data can be scarce due to the T_e^{sep}-based shifting or have large error bars, and the value of R^2 is near zero.

The fits of λ_q with p_e, n_e, and T_e computed at every point along the profiles in Figure 4 can be used to determine the local quantities most strongly correlated with λ_q for shots in all confinement modes (L+I+H, black lines in Figure 4). The scalings with p_e for all modes in the region of $\Psi_N < 0.5$ have the highest R^2 among the local quantity scalings, while the edge T_e at $\rho_{\text{pol}} = 0.95$ ($\Psi_N = 0.90$) somewhat exceeds the R^2 of the p_e fit at the same location. The local n_e fits for all modes have quite low R^2 over the entire profile due to the separate clustering of each confinement mode (not shown). Fits using the average quantities (dashed lines in Figure 4) have higher R^2 than the local p_e fits but similar R^2 compared to those with n_e and T_e. We conclude that the core pressure and to a lesser extent the edge temperature appear to be the most strongly correlated with λ_q across all confinement modes.

The scalings of λ_q in individual confinement modes in Figure 4 show the complicated realities that underlie the scalings for L+I+H mode. The scaling with $\overline{p}$ is the most unified across modes, with the dashed lines in Figure 4(a) having the exponents that are very similar in value. In scalings with n_e and p_e, H-modes have very different exponents compared to L- and I-modes. H-modes also have significantly poorer fits with T_e compared to L- and I-mode. This visualization shows that the scalings of λ_q with local quantities are in all cases less unified across confinement modes than those with average quantities: H-mode scalings with local quantities in particular stand out compared to L- and I-mode, warranting further investigation.

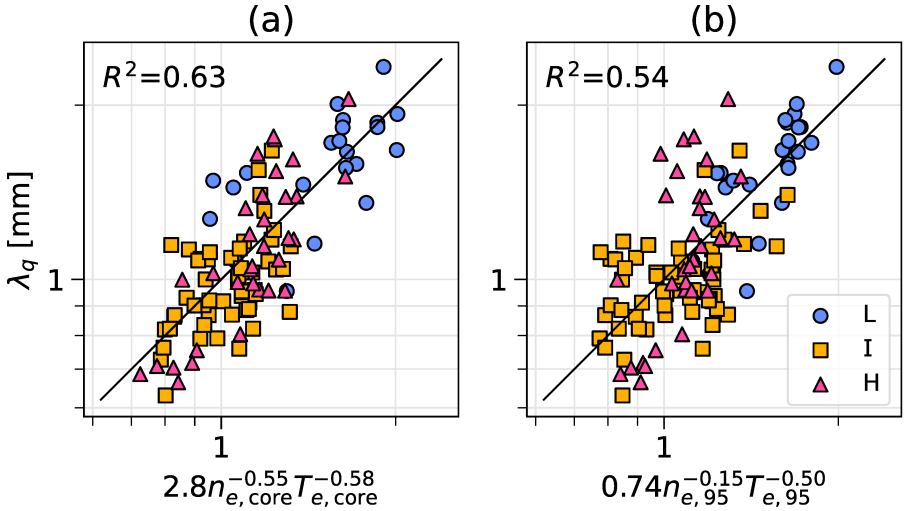

Figure 5: λ_q measurements compared to predictions from the regression $\lambda_q = An_e^bT_e^c$ fit from profiles (a) at $\rho_{pol} \approx 0.1$ and (b) at $\rho_{pol} = 0.95$. The identity line is shown in black.

The importance of p_e^{95} in predicting λ_q is also tested using fits which allow for independent exponents of electron density and temperature ($\lambda_q/\text{mm} = A(n_e/10^{20}\ \text{m}^{-3})^a(T_e/\text{keV})^b$) shown in Figure 5.

In the region of $\rho_{\mathrm{pol}} \approx 0.1$, the n_e and T_e exponents are both around -0.6 (see Figure 5(a) x-axis label), which is close to the $\overline{p}$ scaling exponent of -0.48 (Figure 2(a)), and results in the same R^2 value as the fit with p_e^{core} alone. Further toward the edge, the fit exponent is larger in magnitude for T_e (-0.5) than n_e (-0.15). These two-parameter fits have a higher R^2 in the edge than the fit with p_e^{95} alone (Figure 4(a) black curve), but the low R^2 of the p_e^{95} fit is mainly due to the H-modes having a different slope and less overlap compared to L/I-mode (Figure 2(b)). We conclude from these fits with independent n_e and T_e exponents that near the core, the *pressure* is indeed the important variable to predict λ_q, because n_e and T_e have similar exponents in the optimal fit, while near the edge, the temperature appears to be more important than the pressure.

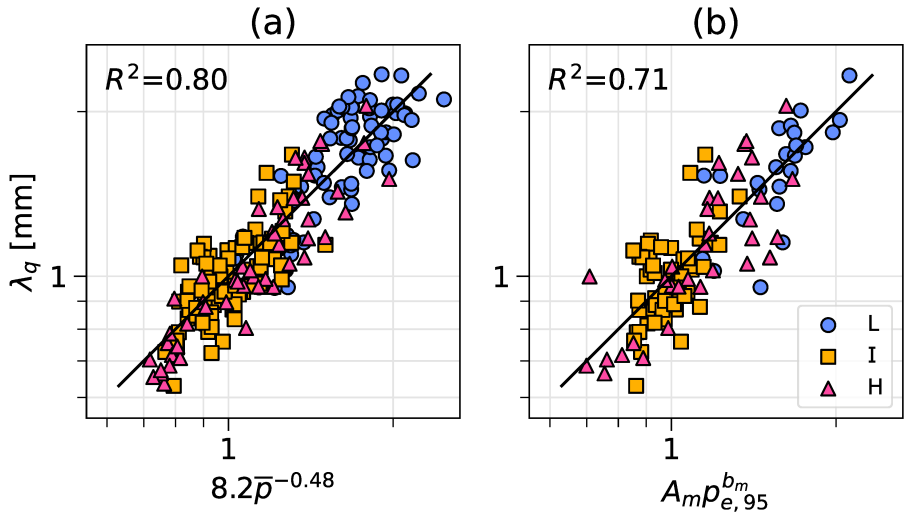

Figure 6: Comparison of the experimental λ_q with (a) λ_q predicted by the Brunner scaling with $\overline{p}$ and (b) λ_q predicted by a mode-dependent fit with p_e at $\rho_{pol} = 0.95$. The identity line is shown in black.

Because the H-modes appear to follow quite a different scaling of λ_q with edge quantities compared to L/I-mode, another option is to abandon the unified scalings and use a different scaling for each confinement mode, i.e. $\lambda_q = A_m p_{e,95}^{b_m}$ where the index m indicates the confinement mode in which the fit was calculated (the values of A and b for each confinement mode are shown in the legend of Figure 2(b)). This mode-dependent fit with $p_{e,95}$ (shown in Figure 6b) results in an R^2 value of 0.71, approaching the quality of the $\overline{p}$ scaling (shown for comparison in Figure 6a). A mode-dependent fit using independent exponents for n_e and T_e at $\rho_{\mathrm{pol}} = 0.95$ ($\lambda_q = A_m n_{e,95}^{b_m} T_{e,95}^{c_m}$) did not provide much improvement, achieving an R^2 value of 0.73. It is therefore possible to achieve accurate predictions of λ_q in C-Mod using edge p_e if the confinement mode is taken into account, and random error in the n_e and T_e profiles does not appear to be responsible for the significantly lower R^2 of the mode-independent p_e^{95} scaling.

λ_q dependence on edge gradients of pressure, temperature, and density

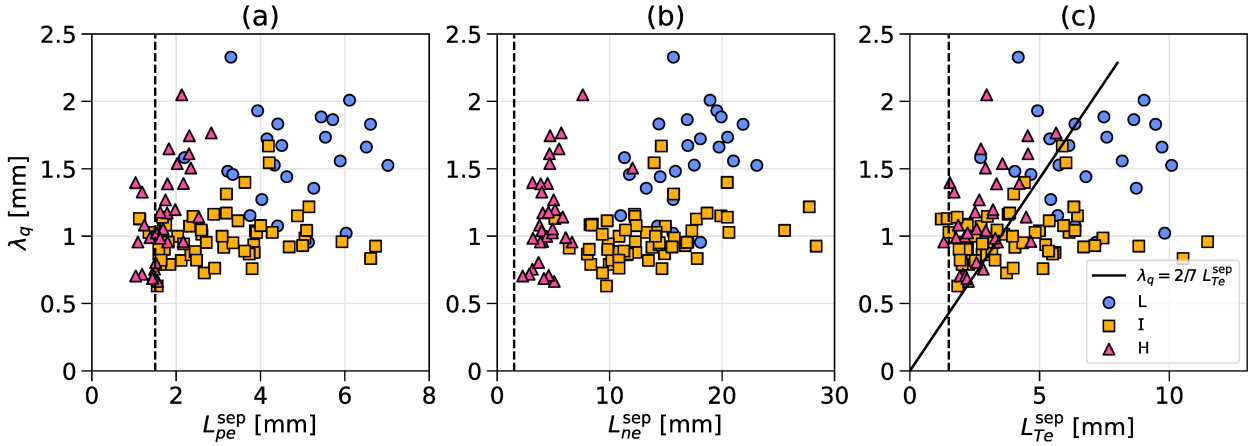

Figure 7: Heat flux width as a function of the gradient length evaluated at the separatrix for (a) electron pressure, (b) electron density, and (c) electron temperature. The solid black line in (c) shows λ_q assuming Spitzer-Härm electron heat conduction. The dashed black vertical lines show the smallest radial feature size of approximately 1.5 mm that can be resolved by Thomson scattering.

In Alcator C-Mod, the heat flux width appears to be overall weakly correlated with separatrix gradient scale lengths (e.g. $L_{Te}^{\text{sep}} = T_e^{\text{sep}}/|\nabla T_e^{\text{sep}}|$), as shown in Figure 7. No single gradient scale length variable appears to have a much stronger correlation with λ_q than the others. Comparing confinement modes, H-modes may have a strong correlation between λ_q and the pressure and density gradient lengths, but there is significant uncertainty in this statement due to the small range of H-mode gradient lengths. L- and I-modes cover a large range of all gradient lengths but show very little correlation with λ_q. The AUG database finds a strong cross-regime correlation between λ_q and λ_{Te}, which are well fit by $\lambda_q = 2/7\ \lambda_{Te}$, the scaling of the Spitzer-Härm electron heat conduction regime. Within individual confinement modes in the AUG database of [14], the Spitzer-Härm scaling is only evident for the L-mode points, but in a different database of AUG H-modes only, the Spitzer-Härm scaling is superior to the flux-limited model [15]. This is different from what is found in the C-Mod database, where the Spitzer-Härm scaling does not adequately characterize any of the individual confinement modes. This may be due to the L-mode data in C-Mod having a maximum L_{Te}^{sep} of 10 mm, while the data in AUG with L_{Te}^{sep} between 10–15 mm are crucial to observe the Spitzer-Härm scaling [14]. H-modes in C-Mod also have smaller L_{Te}^{sep} in the range of 1–6 mm compared to 5–8 mm [14] and 4–11 mm [15] in AUG, and the Spitzer-Härm scaling underestimates λ_q in C-Mod while it overestimates it in AUG [14]. This may be due to C-Mod H-modes having lower collisionality (consistent with steeper temperature gradients), which would result in the Spitzer-Härm scaling being less adequate due to more important kinetic effects, nonlocal transport, and heat flux limiting. This could also explain why the AUG data is better fit by scalings with p_e^{95} and $\lambda_{pe}^{\text{SOL}}$ than the C-Mod data: if the AUG SOL is better characterized by local transport than the C-Mod SOL, AUG would see better correlations of λ_q with local quantities and gradients. We note that one possible source of error in comparing C-Mod and AUG gradient scale lengths is that they are estimated differently. In the AUG analysis, a small region about the separatrix is fit by an exponential with decay length λ_{Te}, with $\lambda_{Te} = L_{Te}^{\text{sep}}$. In contrast, the gradient lengths in the C-Mod database are calculated from the full-profile GPR fits.

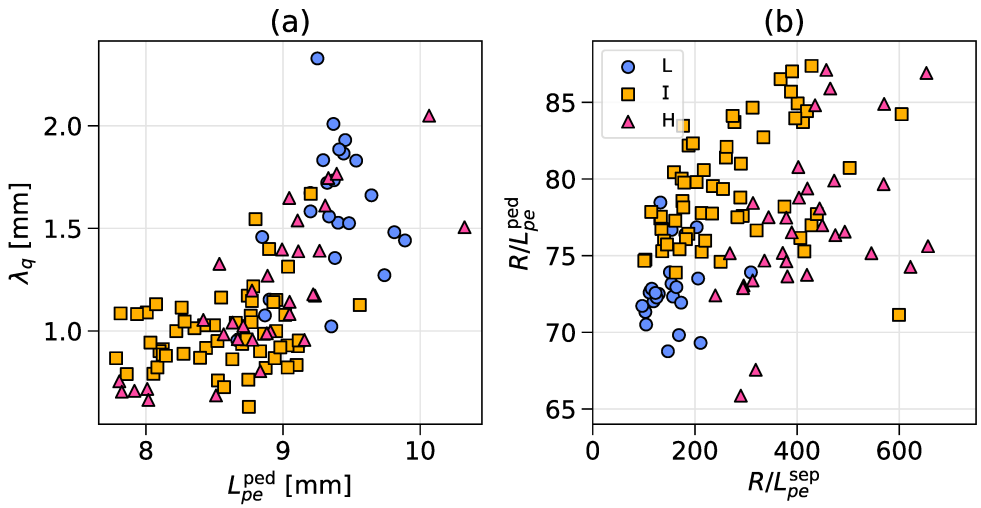

Figure 8: (a) Heat flux width as a function of pedestal electron pressure gradient length. (b) Inverse electron pressure gradient length at the pedestal as a function of inverse electron pressure gradient length at the separatrix, both normalized by major radius ($R = 0.68$ m for C-Mod).

Finally, we examine whether there is a link between λ_q and the pedestal pressure gradient length and look for a relationship between the pedestal and separatrix pressure gradient lengths (Figure 8). The pressure gradient length at the pedestal is defined, for the purpose of comparison to AUG, by the same approximation

$$L_{pe}^{\mathrm{ped}} = -\frac{p_e}{\nabla p_e} \approx \frac{p_e^{95} + p_e^{\mathrm{sep}}}{2} \cdot \frac{R^{\mathrm{sep}} - R^{95}}{p_e^{95} - p_e^{\mathrm{sep}}}$$

[14]. In Figure 8(a) we see a somewhat unified trend between λ_q and L_{pe}^{ped} across all confinement modes, with a similar amount of scatter as in the AUG database. L_{pe}^{ped} appears to be a better predictor of λ_q in C-Mod than L_{pe}^{sep}, at least for L- and I-mode shots (Figure 8(a) compared to Figure 7(a)). In Figure 8(b) we compare the inverse gradient length at the separatrix to the approximate pedestal inverse gradient length, and observe significantly greater spread in the data compared to AUG, with no clear unifying linear trend. This could be due to the much smaller range of R/L_{pe}^{ped} on C-Mod of ~70 to ~85, compared to ~65 to ~125 on AUG [14]. The fact that the pressure gradient in the SOL is somewhat independent of the weakly varying gradient in the pedestal region of the confined plasma may help explain why the scalings of λ_q with p_e^{95} and with L_{pe}^{sep} have more scatter than the scaling with average pressure.

Conclusions

The Alcator C-Mod tokamak heat flux width database, augmented with core and edge electron density, temperature, and pressure profile data, displays a trend of decreasing heat flux width with increasing edge electron pressure, similar to results from the AUG tokamak [14]. Compared to the scaling of λ_q with the average pressure calculated from the total stored energy, however, the absolute value of the exponent is lower and depends on the plasma confinement regime (L-, I-, or H-mode). Therefore, we find that the edge plasma pressure is a worse fit to the heat flux width in C-Mod than the average pressure. We now summarize the results from the analysis of the augmented C-Mod database:

- The scalings with average pressure $\lambda_q/\mathrm{mm} = 8.2(\overline{p}/\mathrm{kPa})^{-0.48}$ (C-Mod [2]) and $\lambda_q/\mathrm{mm} = 7.6(\overline{p}/\mathrm{kPa})^{-0.52}$ (AUG) show good agreement across devices
- The scalings with edge pressure ($\rho_{\mathrm{pol}} = 0.95$) $\lambda_q/\mathrm{mm} = 1.8(p_e^{95}/\mathrm{kPa})^{-0.26}$ (C-Mod) and $\lambda_q/\mathrm{mm} = 2.5(p_e^{95}/\mathrm{kPa})^{-0.34}$ (AUG) are also quite similar, but H-modes in C-Mod have a different trend compared to L- and I-mode
- The core pressure is the local quantity with the highest R^2 when fit to λ_q using data from all confinement regimes

- Fits using p_e^{95} that also depend on the confinement mode approach the high R^2 of the unified fit with $\overline{p}$
- Gradient lengths of electron pressure, density, and temperature at the separatrix have a positive correlation with λ_q, as found in the AUG database, but the Spitzer-Härm scaling of $\lambda_q = 2/7\ \lambda_{Te}$ observed in AUG is not clearly followed in C-Mod
- There is a positive correlation between λ_q and the pedestal pressure gradient length (using values at $\rho_{\mathrm{pol}} = 0.95$ and at the separatrix), as in the AUG database
- There is little correlation between R/L_{pe}^{ped} and R/L_{pe}^{sep} in the C-Mod database, which is different from the strong correlation found in the AUG database

The finding that λ_q is better correlated with $\overline{p}$ in C-Mod than it is with p_e^{95} contrasts with theoretical expectations that cross-field turbulent transport (due to instabilities and modes that strongly depend on local plasma conditions) can broaden the heat load in the SOL [24], while there is as yet no theoretical justification for λ_q to instead be a strong function of the *average* pressure. We therefore list some possible reasons why the scaling with edge pressure in C-Mod is of reduced quality compared to the average pressure:

- The average pressure, being an integrated quantity, can have lower random error than the localized pressure or its gradient
- The edge ion temperature in C-Mod can be significantly higher than the electron temperature, especially at low collisionality [36], which implies that the electron pressure provides an incomplete description compared to the total pressure from stored energy
- There is some error in the EFIT mappings, which use preset functional forms of pressure and other profiles that can lead to inaccuracy in the pedestal top position. Kinetic EFITs, which take experimental profiles into account, could provide an improvement but are unlikely to have a significant impact on quantities other than L_{pe}^{ped}

While the sources of error listed here may explain some differences in fit quality between AUG and C-Mod, they do not explain why H-modes in C-Mod have a clearly different scaling with p_e^{95} than L- and I-mode, which stands as a counterexample to the AUG observation that the scaling with p_e^{95} is universal across all confinement modes.

While the average pressure is a better predictor of the heat flux width in the C-Mod database and the edge pressure does a better job in the AUG database, both of these scalings show some limits: the C-Mod average pressure scaling still has room for improvement when used across different devices [20], and the AUG scaling with edge pressure can be a less good predictor when there is increased filament frequency [25]. Further work is therefore needed for a robust scaling of the heat flux width across different regimes in different devices.

Table 2: Extrapolations of λ_q for ITER and SPARC full-power H-mode scenarios using the C-Mod scalings with average pressure, electron pressure at $\rho_{pol} = 0.95$, and electron pressure at $\rho_{pol} = 0.95$ fitting only the H-mode shots. λ_q values in parentheses indicate that the scaling law was evaluated using the upper limit of the pedestal pressure in SPARC.

Scaling law	ITER λ_q [mm]	SPARC λ_q [mm]
$\boldsymbol{\lambda_q/\mathrm{mm} = 8.2(\overline{p}/\mathrm{kPa})^{-0.48}}$	0.52	0.26
$\boldsymbol{\lambda_q/\mathrm{mm} = 1.8\left(p_e^{95}/\mathrm{kPa}\right)^{-0.26}}$	0.59	0.44 (0.38)
$\boldsymbol{\lambda_q/\mathrm{mm} = 4.6\left(p_e^{95}/\mathrm{kPa}\right)^{-0.55}}$ (H-modes)	0.44	0.23 (0.17)

Finally, we can use the scalings with edge electron pressure from the C-Mod database to extrapolate to estimates for the heat flux width in ITER and SPARC (Table 2). The ITER scenario considered here is the ITER baseline 15 MA, $Q = 10$, inductive H-mode scenario [37] and the SPARC scenario is the 8.7 MA, $Q \approx 11$ H-mode [38]. The predicted profiles for these scenarios are evaluated for the pressure at $\rho_{\mathrm{pol}} = 0.95$ (equivalent to $\rho_{\mathrm{tor}} \approx 0.87$ given the profiles of the rotational transform in the C-Mod database). Using the upper limit of the pedestal pressure in SPARC [39] can provide a lower bound on λ_q (Table 2 values in

parentheses). These extrapolations highlight the importance of preparing for challenging heat flux densities in SPARC and ITER. Results from these two devices should provide crucial data on which of these scalings is most relevant.

Acknowledgements

This work was supported by US DoE Award DE-SC0014264.

Bibliography

[1] Eich T, Leonard A W, Pitts R A, Fundamenski W, Goldston R J, Gray T K, Herrmann A, Kirk A, Kallenbach A, Kardaun O, Kukushkin A S, Labombard B, Maingi R, Makowski M A, Scarabosio A, Sieglin B, Terry J and Thornton A 2013 Scaling of the tokamak near the scrape-off layer H-mode power width and implications for ITER *Nuclear Fusion* **53**

[2] Brunner D, Labombard B, Kuang A Q and Terry J L 2018 High-resolution heat flux width measurements at reactor-level magnetic fields and observation of a unified width scaling across confinement regimes in the Alcator C-Mod tokamak *Nuclear Fusion* **58**

[3] Kuang A Q, Ballinger S, Brunner D, Canik J, Creely A J, Gray T, Greenwald M, Hughes J W, Irby J, LaBombard B, Lipschultz B, Lore J D, Reinke M L, Terry J L, Umansky M, Whyte D G, Wukitch S, and the SPARC Team 2020 Divertor heat flux challenge and mitigation in SPARC *J. Plasma Phys.* **86** 865860505

[4] Lao L L, John H S, Stambaugh R D, Kellman A G and Pfeiffer W 1985 Reconstruction of current profile parameters and plasma shapes in tokamaks *Nucl. Fusion* **25** 1611–22

[5] Leonard A W 2018 Plasma detachment in divertor tokamaks *Plasma Physics and Controlled Fusion* **60**

[6] Valanju P M, Kotschenreuther M, Mahajan S M and Canik J 2009 Super-X divertors and high power density fusion devices *Physics of Plasmas* **16** 056110

[7] Umansky M V, Rensink M E, Rognlien T D, LaBombard B, Brunner D, Terry J L and Whyte D G 2017 Assessment of X-point target divertor configuration for power handling and detachment front control *Nuclear Materials and Energy* 1–6

[8] Reimerdes H, Duval B P, Harrison J R, Labit B, Lipschultz B, Lunt T, Theiler C, Tsui C K, Verhaegh K, Vijvers W A J, Boedo J A, Calabro G, Crisanti F, Innocente P, Maurizio R, Pericoli V, Sheikh U, Spolare M, Vianello N, and and 2017 TCV experiments towards the development of a plasma exhaust solution *Nucl. Fusion* **57** 126007

[9] Morris W, Harrison J R, Kirk A, Lipschultz B, Militello F, Moulton D and Walkden N R 2018 MAST Upgrade Divertor Facility: A Test Bed for Novel Divertor Solutions *IEEE Transactions on Plasma Science* **46** 1217–26

[10] LaBombard B, Marmar E, Irby J, Terry J L, Vieira R, Wallace G, Whyte D G, Wolfe S, Wukitch S, Baek S, Beck W, Bonoli P, Brunner D, Doody J, Ellis R, Ernst D, Fiore C, Freidberg J P, Golfinopoulos T, Granetz R, Greenwald M, Hartwig Z S, Hubbard A, Hughes J W, Hutchinson I H, Kessel C, Kotschenreuther M, Leccacorvi R, Lin Y, Lipschultz B, Mahajan S, Minervini J, Mumgaard R, Nygren R, Parker R, Poli F, Porkolab M, Reinke M L, Rice J, Rognlien T, Rowan W, Shiraiwa S, Terry D, Theiler C, Titus P, Umansky M, Valanju P, Walk J, White A, Wilson J R, Wright G and Zweben S J 2015 ADX: A high field, high power density, advanced divertor and RF tokamak *Nuclear Fusion* **55**

[11] Ryutov D D and Soukhanovskii V A 2015 The snowflake divertor *Physics of Plasmas* **22** 110901

[12] Soukhanovskii V A, Bell R E, Diallo A, Gerhardt S, Kaye S, Kolemen E, LeBlanc B P, McLean A G, Menard J E, Paul S F, Podesta M, Raman R, Rognlien T D, Roquemore A L, Ryutov D D, Scotti F, Umansky M V, Battaglia D, Bell M G, Gates D A, Kaita R, Maingi R, Mueller D and Sabbagh S A 2012 Snowflake divertor configuration studies in National Spherical Torus Experiment *Physics of Plasmas* **19** 082504

[13] Reimerdes H, Canal G P, Duval B P, Labit B, Lunt T, Vijvers W A J, Coda S, Temmerman G D, Morgan T W, Nespoli F and and B T 2013 Power distribution in the snowflake divertor in TCV *Plasma Phys. Control. Fusion* **55** 124027

[14] Silvagni D, Eich T, Faitsch M, Happel T, Sieglin B, David P, Nille D, Gil L, Stroth U, the ASDEX Upgrade team, and the EUROfusion MST1 team 2020 Scrape-off layer (SOL) power width scaling and correlation between

SOL and pedestal gradients across L, I and H-mode plasmas at ASDEX Upgrade *Plasma Phys. Control. Fusion* **62** 045015
[15] Sun H J, Wolfrum E, Eich T, Kurzan B, Potzel S, Stroth U, and the ASDEX Upgrade Team 2015 Study of near scrape-off layer (SOL) temperature and density gradient lengths with Thomson scattering *Plasma Phys. Control. Fusion* **57** 125011
[16] Scarabosio A, Eich T, Herrmann A and Sieglin B 2013 Outer target heat fluxes and power decay length scaling in L-mode plasmas at JET and AUG *Journal of Nuclear Materials* **438** S426–30
[17] Makowski M A, Elder D, Gray T K, Labombard B, Lasnier C J, Leonard A W, Maingi R, Osborne T H, Stangeby P C, Terry J L and Watkins J 2012 Analysis of a multi-machine database on divertor heat fluxes *Physics of Plasmas* **19**
[18] Goldston R J 2011 Heuristic drift-based model of the power scrape-off width in low-gas-puff H-mode tokamaks *Nucl. Fusion* **52** 013009
[19] Goldston R J 2015 Theoretical aspects and practical implications of the heuristic drift SOL model *Journal of Nuclear Materials* **463** 397–400
[20] Horacek J, Adamek J, Komm M, Seidl J, Vondracek P, Jardin A, Guillemaut Ch, Elmore S, Thornton A, Jirakova K, Jaulmes F, Deng G, Gao X, Wang L, Ding R, Brunner D, LaBombard B, Olsen J, Rasmussen J J, Nielsen A H, Naulin V, Ezzat M, Camacho K M, Hron M, Matthews G F, EUROfusion MST1 Team, JET Contributors, and MAST-U Team 2020 Scaling of L-mode heat flux for ITER and COMPASS-U divertors, based on five tokamaks *Nucl. Fusion* **60** 066016
[21] Makowski M A, Lasnier C J, Leonard A W, Osborne T H, Umansky M, Elder J D, Nichols J H, Stangeby P C, Baver D A and Myra J R 2015 Models of SOL transport and their relation to scaling of the divertor heat flux width in DIII-D *Journal of Nuclear Materials* **463** 55–60
[22] Makowski M A, Lasnier C J, Leonard A W and Osborne T H 2017 Analysis of edge stability for models of heat flux width *Nuclear Materials and Energy* **12** 1010–4
[23] Giacomin M, Stagni A, Ricci P, Boedo J A, Horacek J, Reimerdes H and Tsui C K 2021 Theory-based scaling laws of near and far scrape-off layer widths in single-null L-mode discharges *Nucl. Fusion* **61** 076002
[24] Eich T, Manz P, Goldston R J, Hennequin P, David P, Faitsch M, Kurzan B, Sieglin B, Wolfrum E, ASDEX, and EUROfusion b 2020 Turbulence driven widening of the near-SOL power width in ASDEX Upgrade H-Mode discharges *Nucl. Fusion* **60** 056016
[25] Faitsch M, Eich T, Harrer G F, Wolfrum E, Brida D, David P, Griener M and Stroth U 2021 Broadening of the power fall-off length in a high density, high confinement H-mode regime in ASDEX Upgrade *Nuclear Materials and Energy* **26** 100890
[26] Whyte D G, Hubbard A E, Hughes J W, Lipschultz B, Rice J E, Marmar E S, Greenwald M, Cziegler I, Dominguez A, Golfinopoulos T, Howard N, Lin L, McDermott R M, Porkolab M, Reinke M L, Terry J, Tsujii N, Wolfe S, Wukitch S, Lin Y, and the Alcator C-Mod Team 2010 I-mode: an H-mode energy confinement regime with L-mode particle transport in Alcator C-Mod *Nucl. Fusion* **50** 105005
[27] Greenwald M, Boivin R, Bonoli P, Budny R, Fiore C, Goetz J, Granetz R, Hubbard A, Hutchinson I, Irby J, LaBombard B, Lin Y, Lipschultz B, Marmar E, Mazurenko A, Mossessian D, Sunn Pedersen T, Pitcher C S, Porkolab M, Rice J, Rowan W, Snipes J, Schilling G, Takase Y, Terry J, Wolfe S, Weaver J, Welch B and Wukitch S 1999 Characterization of enhanced Dα high-confinement modes in alcator *C*-mod *Physics of Plasmas* **6** 1943–9
[28] Snipes J A, LaBombard B, Greenwald M, Hutchinson I H, Irby J, Lin Y, Mazurenko A and Porkolab M 2001 The quasi-coherent signature of enhanced Dα H-mode in Alcator C-Mod *Plasma Phys. Control. Fusion* **43** L23–30
[29] LaBombard B, Golfinopoulos T, Terry J L, Brunner D, Davis E, Greenwald M and Hughes J W 2014 New insights on boundary plasma turbulence and the quasi-coherent mode in Alcator C-Mod using a Mirror Langmuir Probe *Physics of Plasmas* **21** 056108
[30] Hughes J W, Mossessian D, Zhurovich K, DeMaria M, Jensen K and Hubbard A 2003 Thomson scattering upgrades on Alcator C-Mod *Review of Scientific Instruments* **74** 1667–70
[31] Basse N P, Dominguez A, Edlund E M, Fiore C L, Granetz R S, Hubbard A E, Hughes J W, Hutchinson I H, Irby J H, LaBombard B, Lin L, Lin Y, Lipschultz B, Liptac J E, Marmar E S, Mossessian D A, Parker R R, Porkolab M, Rice

J E, Snipes J A, Tang V, Terry J L, Wolfe S M, Wukitch S J, Zhurovich K, Bravenec R V, Phillips P E, Rowan W L, Kramer G J, Schilling G, Scott S D and Zweben S J 2007 Diagnostic Systems on Alcator C-Mod *Fusion Science and Technology* **51** 476–507

[32] Chilenski M A, Greenwald M, Marzouk Y, Howard N T, White A E, Rice J E and Walk J R 2015 Improved profile fitting and quantification of uncertainty in experimental measurements of impurity transport coefficients using Gaussian process regression *Nucl. Fusion* **55** 023012

[33] Hughes J W, Mossessian D A, Hubbard A E, Marmar E S, Johnson D and Simon D 2001 High-resolution edge Thomson scattering measurements on the Alcator C-Mod tokamak *Review of Scientific Instruments* **72** 1107–10

[34] Hughes J W, Mossessian D A, Hubbard A E, LaBombard B and Marmar E S 2002 Observations and empirical scalings of the high-confinement mode pedestal on Alcator C-Mod *Physics of Plasmas* **9** 3019–30

[35] Stangeby 2000 *The Plasma Boundary of Magnetic Fusion Devices* (Bristol: Institute of Physics Publishing)

[36] Brunner D, Labombard B, Churchill R M, Hughes J, Lipschultz B, Ochoukov R, Rognlien T D, Theiler C, Walk J, Umansky M V and Whyte D 2013 An assessment of ion temperature measurements in the boundary of the Alcator C-Mod tokamak and implications for ion fluid heat flux limiters *Plasma Physics and Controlled Fusion* **55**

[37] Casper T, Gribov Y, Kavin A, Lukash V, Khayrutdinov R, Fujieda H, Kessel C, ITER Organization, and ITER Domestic Agencies 2014 Development of the ITER baseline inductive scenario *Nucl. Fusion* **54** 013005

[38] Rodriguez-Fernandez P, Howard N T, Greenwald M J, Creely A J, Hughes J W, Wright J C, Holland C, Lin Y and Sciortino F 2020 Predictions of core plasma performance for the SPARC tokamak *Journal of Plasma Physics* 1–24

[39] Hughes J W, Howard N T, Rodriguez-Fernandez P, Creely A J, Kuang A Q, Snyder P B, Wilks T M, Sweeney R and Greenwald M 2020 Projections of H-mode access and edge pedestal in the SPARC tokamak *J. Plasma Phys.* **86** 865860504